


ORIGINAL ARTICLE

Predicting microvascular invasion in hepatocellular carcinoma: A dual-institution study on gadoxetate disodium-enhanced MRI

Hanyu Jiang¹  | Jingwei Wei^{2,3} | Fangfang Fu^{4,5} | Hong Wei¹ | Yun Qin¹ | Ting Duan¹ | Weixia Chen¹ | Kunlin Xie⁶ | Jeong Min Lee⁷ | Mustafa R. Bashir^{8,9,10} | Meiyun Wang^{4,5} | Bin Song¹ | Jie Tian^{2,3,11,12,13} 

¹Department of Radiology, West China Hospital, Sichuan University, Chengdu, Sichuan, China

²Key Laboratory of Molecular Imaging, Institute of Automation, Chinese Academy of Sciences, Beijing, China

³Beijing Key Laboratory of Molecular Imaging, Beijing, China

⁴Department of Medical Imaging, Henan Provincial People's Hospital, Zhengzhou, China

⁵Department of Medical Imaging, People's Hospital of Zhengzhou University, Zhengzhou, China

⁶Department of Liver Surgery & Liver Transplantation, West China Hospital, Sichuan University, Chengdu, China

⁷Department of Radiology, Seoul National University Hospital and Seoul National University College of Medicine, Seoul, South Korea

⁸Department of Radiology, Duke University Medical Center, Durham, North Carolina, USA

⁹Center for Advanced Magnetic Resonance in Medicine, Duke University Medical Center, Durham, North Carolina, USA

¹⁰Division of Gastroenterology, Department of Medicine, Duke University Medical Center, Durham, North Carolina, USA

¹¹Beijing Advanced Innovation Center for Big Data-Based Precision Medicine, School of Medicine, Beihang University, Beijing, China

¹²Engineering Research Center of Molecular and Neuro Imaging of Ministry of Education, School of Life Science and Technology, Xidian University, Xi'an, China

¹³Key Laboratory of Big Data-Based Precision Medicine (Beihang University), Ministry of Industry and Information Technology, Beijing, China

Correspondence

Meiyun Wang, Department of Medical Imaging, Henan Provincial People's Hospital, Zhengzhou, Henan, 450003, China.
Email: mywang@ha.edu.cn

Bin Song, Department of Radiology, West China Hospital, Sichuan University, Chengdu, Sichuan, 610041, China.
Email: anicesong@vip.sina.com

Jie Tian, Key Laboratory of Molecular Imaging, Institute of Automation, Chinese Academy of Sciences, Beijing 100190, China.
Email: jie.tian@ia.ac.cn

Funding information

This study was funded by the National Natural Science Foundation of China

Abstract

Background & Aims: Microvascular invasion (MVI) is an important risk factor in hepatocellular carcinoma (HCC), but its diagnosis mandates postoperative histopathologic analysis. We aimed to develop and externally validate a predictive scoring system for MVI.

Methods: From July 2015 to November 2020, consecutive patients underwent surgery for HCC with preoperative gadoxetate disodium (EOB)-enhanced MRI was retrospectively enrolled. All MR images were reviewed independently by two radiologists who were blinded to the outcomes. In the training centre, a radio-clinical MVI score was developed via logistic regression analysis against pathology. In the testing centre, areas under the receiver operating curve (AUCs) of the MVI score and other previous MVI schemes were compared. Overall survival (OS) and recurrence-free survival (RFS) were analysed by the Kaplan–Meier method with the log-rank test.

Abbreviations: AFP, alpha-fetoprotein, AUC, area under the receiver operating curve, DWI, diffusion-weighted imaging, EOB, gadoxetate disodium, HBP, hepatobiliary phase, HCC, hepatocellular carcinoma, MVI, microvascular invasion, OR, odds ratio, OS, overall survival, RFS, recurrence-free survival.

Hanyu Jiang, Jingwei Wei, and Fangfang Fu contributed equally to this work.

This is an open access article under the terms of the Creative Commons Attribution-NonCommercial-NoDerivs License, which permits use and distribution in any medium, provided the original work is properly cited, the use is non-commercial and no modifications or adaptations are made.

© 2022 The Authors. *Liver International* published by John Wiley & Sons Ltd.

(Grant nos. 82101997, 62027901, 81227901, 81930053, 82001917), the Science and Technology Support Program of Sichuan Province (grant no. 2021YFS0141 and 2021YFS0021), Ministry of Science and Technology of China (grant no. 2017YFA0205200), The Project of High-Level Talents Team Introduction in Zhuhai City (grant no. Zhuhai HLHPTP201703). The authors would like to acknowledge the instrumental and technical support of the Multimodal Biomedical Imaging Experimental Platform, Institute of Automation, Chinese Academy of Sciences.

Handling Editor: Alejandro Forner

Results: A total of 417 patients were included, 195 (47%) with pathologically-confirmed MVI. The MVI score included: non-smooth tumour margin (odds ratio [OR] = 4.4), marked diffusion restriction (OR = 3.0), internal artery (OR = 3.0), hepatobiliary phase peritumoral hypointensity (OR = 2.5), tumour multifocality (OR = 1.6), and serum alpha-fetoprotein >400 ng/mL (OR = 2.5). AUCs for the MVI score were 0.879 (training) and 0.800 (testing), significantly higher than those for other MVI schemes (testing AUCs: 0.648–0.684). Patients with model-predicted MVI had significantly shorter OS (median 61.0 months vs not reached, $P < .001$) and RFS (median 13.0 months vs 42.0 months, $P < .001$) than those without.

Conclusions: A preoperative MVI score integrating five EOB-MRI features and serum alpha-fetoprotein level could accurately predict MVI and postoperative survival in HCC. Therefore, this score may aid in individualized treatment decision making.

KEYWORDS

diagnosis, gadoxetate disodium-enhanced MRI, hepatocellular carcinoma, microvascular invasion, survival

1 | INTRODUCTION

Microvascular invasion (MVI) is associated with a more aggressive biologic behaviour in hepatocellular carcinoma (HCC) and is an important risk factor for postoperative recurrence and reduced survival.^{1–5} MVI has been reported in around 15%–57% of HCCs,^{3–7} and detection of MVI in the pre-treatment stage is critical for proper therapeutic decision-making, for example, for selection of surgery over ablation,⁴ wider resection margins at hepatectomy, closer monitoring of tumour progression^{3,5} and potential use of adjuvant therapies. However, diagnosis of MVI currently requires histopathologic analysis of the surgical specimens, which is subject to sampling errors and can only be achieved postoperatively.^{3–5}

As a result, identifying reproducible and accurate preoperative predictors for MVI has become a recent area of active research.^{4,6,8–20} Prior works explored the utility of certain laboratory^{8–10} and imaging findings (e.g. non-smooth tumour margin, arterial phase peritumoral enhancement, hepatobiliary phase [HBP] peritumoral hypointensity on gadoxetate disodium [EOB]-enhanced MRI, etc.)^{4,6,8,11–20} for preoperative MVI prediction. Although easy to use, most of these studies assessed a limited number of predictors in a relatively small single-centre cohort and demonstrated varied predictive accuracies, and thus not yet ready to be incorporated into routine clinical practice.

On the contrary, promising results have been reported with the implementation of preoperative CT or MRI-based artificial intelligence techniques for MVI detection, with an area under the receiver operating curve (AUC) reaching up to 0.812–0.889.^{21–24} Nevertheless, limited interpretability, reproducibility, and generalizability may dampen confident clinical adoptions. Furthermore, the lack of external validation prevents reliable conclusions from being

Lay Summary

1. In patients with hepatocellular carcinoma, five gadoxetate disodium-enhanced MR imaging features (non-smooth tumour margin, marked diffusion restriction, internal artery, hepatobiliary phase peritumoral hypointensity, and tumour multifocality), and serum alpha-fetoprotein >400 ng/mL were significantly associated with microvascular invasion (MVI).
2. An MVI score based on the above predictors demonstrated significantly superior diagnostic performance (testing centre AUC: 0.800) than previously reported MVI schemes (testing centre AUC: 0.648–0.684) and achieved accurate postoperative survival stratification.

drawn.^{21–23} Therefore, the imaging criteria for MVI remain a matter of debate.

Thus, this dual-institution study aimed to propose and externally validate an easy-to-use scoring system based on clinical and EOB-MRI features for preoperative MVI prediction and to evaluate its ability to stratify postoperative survival in HCC patients.

2 | PATIENTS AND METHODS

This retrospective, dual-centre study was approved by the institutional review boards at West China Hospital, Sichuan University (termed the 'training centre') and Henan Provincial People's Hospital (termed the 'testing centre'). The requirements for informed consent were waived.

2.1 | Patients

From July 2015 to November 2020, consecutive patients who met the following inclusion criteria were enrolled: (a) surgically confirmed HCC; (b) pathologically documented MVI status; (c) underwent preoperative EOB-MRI. Patients were excluded if (a) they had any previous treatment for HCC; (b) the EOB-MRI examinations were not performed within 1 month prior to surgery; (c) the pathology report was inadequate for the determination of MVI status; (d) key laboratory results (detailed below) within 2 weeks prior to surgery were not available; (e) the MR images were of inadequate quality for image analysis. According to the *rule of thumb* for sample size calculation, at least 5–10 outcome events per variable is suggested for effective modelling.²⁵ Therefore, patients with macrovascular invasion at imaging were retained in the training centre dataset to guarantee adequate positive cases for model construction. However, these patients were excluded from the testing centre dataset to avoid over-estimation of model performances. Patient inclusion/exclusion is illustrated in Figure 1.

Baseline clinical data, including patient demographics, underlying liver diseases, presence or absence of cirrhosis, and Barcelona Clinic Liver Cancer (BCLC) stages were recorded. Key laboratory results, including serum alpha-fetoprotein (AFP), alanine aminotransferase (ALT), aspartate aminotransferase (AST), total bilirubin (TBIL), albumin (ALB) and platelet count (PLT), were recorded.

2.2 | EOB-MRI Acquisition

All EOB-MR images were acquired on one of two 3.0 T MR systems (Magnetom Skyra, Siemens Healthineers; Discovery MR 750, GE Healthcare). All EOB-MRI examinations were performed with comparable, clinically appropriate liver protocols at the training and testing centres, including: T2-weighted imaging; diffusion-weighted

imaging (DWI) with apparent diffusion coefficient (ADC) maps; T1-weighted imaging before and after injection of EOB in the late arterial phase (AP), portal venous phase (PVP), transitional phase and HBP. The EOB-MRI acquisition protocols are detailed in Material S1.

2.3 | Image Analysis

All deidentified MR images were transmitted to the training centre and reviewed centrally by two fellowship-trained abdominal radiologists (with 5 and 7 years of experience in liver MRI, respectively) who were blinded to all patient clinical, pathologic and follow-up information. All disagreements between the reviewers were resolved by a third senior radiologist who had over 20 years of experience in liver MRI.

On a per-patient basis, the reviewers independently evaluated imaging features which had been reported to correlate with MVI, tumour burden, and HCC biological behaviours, including: (a) number of tumours defined according to the BCLC algorithm (solitary vs. 2–3 and over 3 tumours)¹; (b) presence or absence of LI-RADS version 2018 major and ancillary features (except for those related to growth or ultrasound visibility since these were not available)²⁶; (c) presence or absence of imaging features profiling peritumoral alterations, including PVP peritumoral hypointensity, HBP peritumoral hypointensity, and peritumoral biliary ductal dilation^{4,6,11,14} and (d) other imaging features of interest, including HCC growth subtypes (single nodular vs. single nodular with extranodular growth vs. confluent multinodular),²⁷ presence or absence of bilobar involvement, internal artery,^{13,28} the two-trait predictor of venous invasion (TTPVI),¹³ complete vs. disrupted “capsule”,⁸ and non-smooth tumour margin.^{13,14} Detailed definitions and typical cases of the imaging features are presented in Material S2. In patients with multiple lesions, the largest lesion was selected for feature-related analyses.

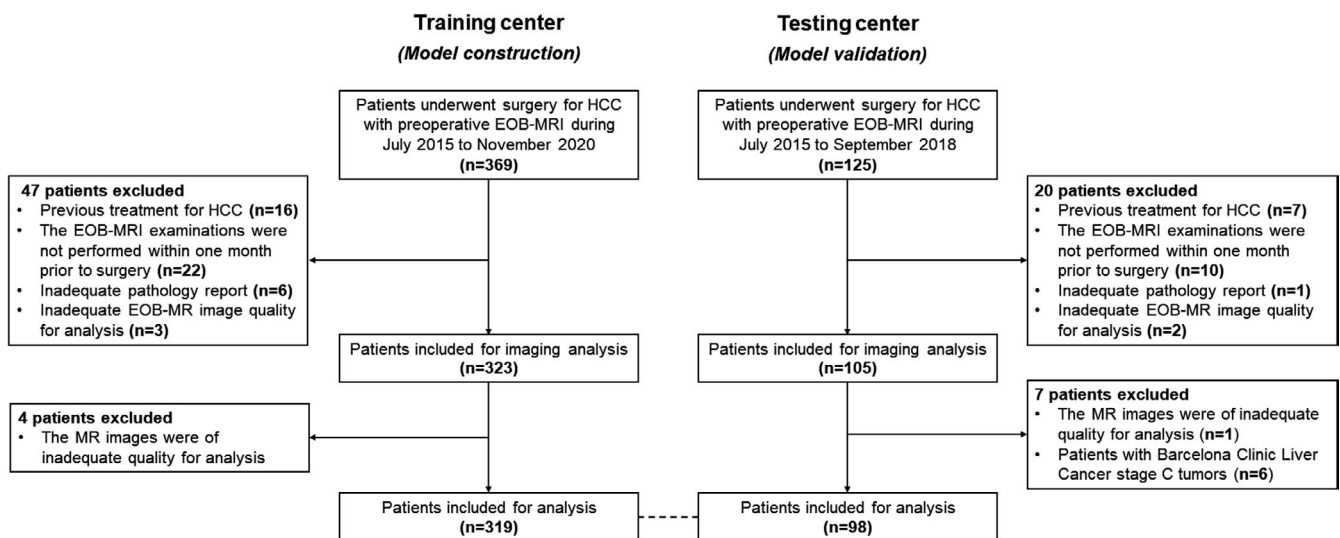


FIGURE 1 Study flow chart

2.4 | Reference Standard

Histopathologic data from routine reports were retrieved as the reference standard for determining MVI status. As per the institutional standard practice procedure, two liver pathologists who were aware of the clinical and imaging data at each centre reviewed all surgical specimens in consensus. MVI was defined as the presence of tumour thrombi within small peritumoral vessels on microscopy via a standard seven-site sampling approach.²⁹

2.5 | Follow-up

Clinical follow-up data were available for the training centre but not for the testing centre. Patients were followed up after surgery at 1 month, every 3 months for the first 2 years, and every 6 months thereafter with serum AFP and contrast-enhanced ultrasound, CT, or MRI. Recurrence was defined as the radiological identification of local/regional disease or distant metastasis. Patients were followed up until death or the last follow-up date (20 January 2021), whichever occurred first, and overall survival (OS) and recurrence-free survival (RFS) were calculated.

2.6 | Statistical Analysis

Differences in baseline clinical, laboratory and radiological data were compared using either Student's *t* test or the Mann–Whitney *U* test for continuous variables, and either chi-squared test or the Fisher's exact test for categorical variables, as appropriate.

2.6.1 | Assessment of the inter-rater agreement

Inter-rater agreement between the two reviewers was measured by computing the intraclass correlation coefficient (ICC) for continuous variables, Cohen's κ value for binary imaging features, and weighted κ value for categorical imaging features, respectively.

2.6.2 | Development and validation of the MVI score

The MVI score was developed from the training centre data based on consensus interpretations of the two reviewers and validated externally in the testing centre based on per-reader and consensus data. Sample size estimation was based on the *rule of thumb*,²⁵ thus the maximum number of variables allowed in the multivariable logistic regression analysis was determined according to 20% of MVI-positive cases in the training centre.

In specific, using the training centre data, univariable logistic regression analysis was conducted to identify significant clinical, laboratory, and radiological predictors, whilst adjusting for patient age and gender. To improve the clinical utility, continuous variables were

converted to categorical or dichotomized variables according to ranges of normality or clinical relevance. For predictors which were collinear based on pairwise Spearman's correlation analysis, those with the largest odds ratios were chosen for further analyses.

Then, controlling for age and gender, all significant predictors from the above steps were fit into a multivariable logistic regression model using the backward stepwise method with fivefold cross-validation, and the Akaike Information Criterion was used to obtain the most parsimonious feature combination. A MVI scoring system was then derived based on the significant predictors at multivariable analysis weighted by their regression coefficients, with the largest regression coefficient scaled as 10 points. The optimal threshold of the scoring system for predicting MVI was determined by receiver operating characteristic analysis with the Youden's index.

Additionally, patients with different MVI scores were stratified into three groups based on the associated likelihood of MVI (<40% as low risk, $\geq 90\%$ as high-risk, and the remainder as medium-risk). A high sensitivity model (with the threshold of MVI score set based on the low-risk group) and a high specificity model (with the threshold of MVI score set based on the high-risk group) was developed accordingly.

Diagnostic performances were computed and compared between the MVI score and other MVI prediction systems proposed by Renzulli et al.,¹³ Min et al.,⁶ and Lee et al.¹⁴ with the area under the receiver operating characteristic curve (AUC), sensitivity, specificity, positive predictive value (PPV), negative predictive value (NPV), and accuracy. Pairwise sensitivities, specificities, and accuracies were compared with the McNemar's test, whilst AUCs were compared using the Delong test. Subgroup analyses in patients with BCLC 0/A stage tumours and BCLC B stage tumours were conducted.

2.6.3 | Survival analysis

Using the training centre data, survival analyses were performed in patients without active malignancies or metastases other than HCC who had complete follow-up information. Kaplan–Meier curves were plotted to analyse survival outcomes, with the log-rank test to assess statistical significance. Multivariable survival analysis was conducted with Cox proportional hazard model whilst adjusted for patient age and gender. *P*-values for multiple comparisons were corrected by the Bonferroni test.

All analyses were performed with R software (version 3.5.1; R Foundation for Statistical Computing). Two-tailed $P \leq .05$ was considered statistically significant.

3 | RESULTS

3.1 | Patients

A total of 417 HCC patients (343 men; 53.2 ± 11.3 years) were included, with 319 (76%) and 98 (24%) patients enrolled from the training and testing centres, respectively. MVI was pathologically

confirmed in 151 (47%) patients from the training centre and in 44 (45%) patients from the testing centre.

Patients from the training centre were slightly younger than those from the testing centre (mean age, 52.6 years vs. 55.1 years, $P = .049$). The median size of HCC in the training centre data was significantly larger than that in the testing centre data (4.3 cm vs. 3.2 cm, $P < .001$). More patients from the training centre had chronic hepatitis (92% vs. 81%, $P = .002$), whilst more patients from the testing centre had established cirrhosis (49% vs. 63%, $P = .01$). High serum AFP level of >400 ng/mL was more frequently detected in patients from the training centre (29% vs. 18%, $P = .04$), whilst TBIL elevation was more frequently detected in patients from the testing centre (3% vs. 34%, $P < .001$). There was no difference in MVI incidence ($P = .67$) or other clinical characteristics between the training and testing centres ($P = .15$ to $.82$).

Key clinical characteristics are summarized in Table 1. Frequencies and inter-rater agreement of imaging features are detailed in Material S3.

3.2 | Development and validation of the MVI score

3.2.1 | Development of the MVI score in the training centre

Using the training centre data, BCLC stage, three laboratory variables (serum AFP, AST and PLT), and 19 imaging variables were significantly associated with MVI at univariable analysis (Table 2).

At multivariable analysis, serum AFP > 400 ng/mL (OR = 2.5 [95% CI: 1.3–5.0], $P = .009$) and five imaging variables, including non-smooth tumour margin (absent vs. present; OR = 4.4 [95% CI: 2.2–8.6], $P < .001$), marked diffusion restriction (absent vs. present; OR = 3.0 [95% CI: 1.7–5.5], $P < .001$), internal artery (absent vs. present; OR = 3.0 [95% CI: 1.5–5.9], $P = .002$), HBP peritumoral hypointensity (absent vs. present; OR = 2.5 [95% CI: 1.3–4.8], $P = .007$), and number of tumours (solitary vs. 2–3 vs. over 3; OR = 1.6 [95% CI: 1.1–2.5], $P = .03$) were significantly associated with MVI. Based on these predictors, the MVI score was constructed as illustrated in Figure 2. EOB-MR images of a representative case with MVI are shown in Material S4.

3.2.2 | Development of the MVI risk system and diagnostic models in the training centre

According to Youden's index, the optimal threshold for predicting MVI was 20 points. Based on the pre-defined criteria for stratifying MVI risks, patients with the MVI scores ≤ 12 points were categorized as low-risk, those with the MVI scores between 12 and 26 points as medium-risk, and those with the MVI scores >26 points as high-risk (Material S5).

Three diagnostic models were generated using these thresholds: an optimal model (threshold >20 points); a high sensitivity model

(threshold >12 points); and a high specificity model (threshold >26 points).

3.2.3 | Training centre performances for MVI

For the training centre data, inter-rater agreement was substantial (ICC: 0.799, [95%CI: 0.750–0.839]) for the MVI score, and moderate for the optimal model (Cohen's κ : 0.512 [95%CI: 0.418–0.607]), the high sensitivity model (Cohen's κ : 0.418 [95%CI: 0.315–0.523]), and the high specificity model (Cohen's κ : 0.567 [95%CI: 0.469–0.665]).

Based on consensus interpretations of the two reviewers, the MVI risk in the low, medium, and high-risk groups was 12% (15/122), 47% (51/108), and 96% (85/89), respectively. The MVI score demonstrated an AUC of 0.879 (95%CI: 0.838–0.913). The optimal model yielded a sensitivity of 72%, specificity of 86%, and accuracy of 80% for predicting MVI, respectively. These values were 90%, 64% and 76% for the high sensitivity model, and 56%, 98% and 78% for the high specificity model, respectively.

3.2.4 | Testing centre performances for MVI

For the testing centre data, inter-rater agreement was substantial (ICC: 0.750 [95%CI: 0.627 to 0.832]) for the MVI score, and moderate for the optimal model (Cohen's κ : 0.481 [95%CI: 0.290–0.671]), the high sensitivity model (Cohen's κ : 0.455 [95%CI: 0.282–0.628]) and the high specificity model (Cohen's κ : 0.560 [95%CI: 0.313–0.801]).

Based on consensus interpretations of the two reviewers, the MVI risk in the low, medium, and high-risk groups was 16% (5/32), 50% (27/54) and 100% (12/12), respectively. The AUC of the MVI score in the entire testing centre cohort, patients with BCLC O/A tumours, and BCLC-B patients was 0.800 (95% CI: 0.707–0.874), 0.726 (95% CI: 0.609–0.824) and 0.875 (95% CI: 0.682–0.972), respectively. In the entire testing centre cohort, the optimal model yielded a sensitivity of 52%, specificity of 89% and accuracy of 72% for predicting MVI, respectively; these values were 89%, 50% and 67% for the high sensitivity model, and 27%, 100% and 67% for the high specificity model, respectively.

Testing centre diagnostic performances of the MVI score and previously reported MVI models based on consensus data are summarized in Table 3, and those based on per-reader data are presented in Material S6.

3.2.5 | Testing centre comparisons with existing MVI predictive schemes

Based on the entire testing centre cohort data, the MVI score demonstrated significantly higher AUC (0.800, 95% CI: 0.707–0.874) than the models proposed by Renzulli et al. (0.648, 95%

TABLE 1 Baseline clinical characteristics of patients

Characteristics	Training centre				Testing centre			
	All	MVI-positive	MVI-negative	P value ^a	All	MVI-positive	MVI-negative	P value ^a
No. patients	319	151 (47)	168 (53)	—	98	44 (45)	54 (55)	—
Age (years)	52.6 ± 11.6	51.7 ± 11.9	53.4 ± 11.3	.20	55.1 ± 10.0	54.9 ± 10.8	55.3 ± 9.3	.73
Gender								
Men	260 (82)	120	140	.38	83 (85)	36	47	.48
Women	59 (18)	31	28		15 (15)	8	7	
Underlying liver diseases								
Chronic hepatitis B	293 (92)	139	154	.66	79 (81)	33	46	.42
Chronic hepatitis C	7 (2)	3	4		4 (4)	2	2	
Chronic hepatitis B and C	4 (1)	3	1		0 (0)	0	0	
Others	15 (5)	6	9		15 (15)	9	6	
Cirrhosis	156 (49)	66	90	.08	62 (63)	20	42	.001
Tumour size ^b (cm)	4.3 (2.4–7.1)	6.5 (3.4–9.0)	3.2 (2.0–4.8)	<.001	3.2 (2.1–4.6)	4.5 (3.5–6.0)	2.3 (1.8–3.2)	<.001
Tumour number								
Solitary	194 (61)	64	130	<.001	62 (63)	21	41	.001
2–3 tumours	70 (22)	39	31		21 (21)	11	10	
>3 tumours	55 (17)	48	7		15 (15)	12	3	
Barcelona Clinic Liver Cancer stage								
0	50 (16)	10	40	<.001	17 (17)	2	15	<.001
A	138 (43)	46	92		56 (57)	22	34	
B	61 (19)	35	26		25 (26)	20	5	
C	70 (22)	60	10		0 (0)	0	0	
Laboratory variables								
AFP (ng/mL)								
≤400	227 (71)	83	144	<.001	80 (82)	33	47	.13
>400	92 (29)	68	24		18 (18)	11	7	
TBIL (μmol/L)								
≤40	311 (98)	144	167	.02	65 (66)	31	34	.44
>40	8 (3)	7	1		33 (34)	13	20	
ALT (U/L)								
≤40	186 (58)	85	101	.49	59 (60)	25	34	.54
>40	133 (42)	66	67		39 (40)	19	20	
AST (U/L)								
≤35	162 (51)	63	99	.002	58 (59)	21	37	.04
>35	157 (49)	88	69		40 (41)	23	17	
ALB (g/L)								
≥40	238 (75)	111	127	.68	76 (78)	38	38	.06
<40	81 (25)	40	41		22 (22)	6	16	
Platelet, 10 ⁹ /L								
≥125	180 (56)	97	83	.008	54 (55)	24	30	.92
<125	139 (44)	54	85		44 (45)	20	24	

Note: Unless stated otherwise, data in parentheses are percentages or interquartile ranges, as appropriate. Two-tailed $P \leq .05$ was considered statistically significant and shown in bold.

Abbreviations: AFP, alpha-fetoprotein; ALB, albumin; ALT, alanine aminotransferase; AST, aspartate aminotransferase; MVI, microvascular invasion; TBIL, total bilirubin.

^aDifferences were compared between MVI-positive and MVI-negative patients using either Student's t test or the Mann–Whitney U test for continuous variables, and χ^2 test or the Fisher's exact test for categorical variables, as appropriate.

^bIn patients with multiple tumours, the sizes of the largest tumours were presented.

TABLE 2 Potential predictors for microvascular invasion in the training centre

Predictors	Univariable analysis		Multivariable analysis			
	Odds ratio (95% CI)	P value	Odds ratio (95%CI)	Regression coefficient	P value	MVI score points (negative/positive)
Clinical predictors						
BCLC stage (0, A, B and C)	2.9 (2.2–3.9)	<.001	–	–	–	–
Laboratory predictors						
AFP (≤ 400 vs > 400 ng/mL)	4.9 (2.9–5.4)	<.001	2.5 (1.3–5.0)	0.92	0.009	0/6
AST (≤ 35 vs > 35 U/L)	2.0 (1.3–3.1)	.003	–	–	–	–
PLT (≥ 125 vs < 125 $10^9/L$)	0.55 (0.35–0.87)	.01	–	–	–	–
Imaging predictors						
No. tumours (Solitary, 2–3, over 3)	3.3 (2.3–4.7)	<0.001	1.6 (1.1–2.5)	0.49	0.03	0/3/7 ^a
Size (cm)	3.3 (2.3–4.7)	<0.001	–	–	–	–
Corona enhancement (absent vs present)	6.0 (3.6–9.8)	<0.001	–	–	–	–
Fat in mass, more than adjacent liver (absent vs present)	0.4 (0.3–0.7)	<0.001	–	–	–	–
Nodule-in-nodule (absent vs present)	1.7 (1.1–2.7)	.03	–	–	–	–
Mosaic architecture (absent vs present)	5.9 (3.6–9.5)	<0.001	–	–	–	–
Blood products in mass (absent vs present)	3.9 (2.5–6.3)	<0.001	–	–	–	–
Tumour in vein (absent vs present)	9.9 (4.8–20.2)	<0.001	–	–	–	–
Marked diffusion restriction (absent vs present)	4.4 (2.7–7.0)	<0.001	3.0 (1.7–5.5)	1.11	<.001	0/7
Infiltrative appearance (absent vs present)	8.5 (4.2–17.6)	<0.001	–	–	–	–
Necrosis or severe ischemia (absent vs present)	3.0 (1.8–4.9)	<0.001	–	–	–	–
Portal venous phase peritumoral hypointensity (absent vs present) ^b	6.0 (3.6–10.0)	<0.001	–	–	–	–
Hepatobiliary phase peritumoral hypointensity (absent vs present) ^b	6.9 (4.2–11.5)	<0.001	2.5 (1.3–4.8)	0.90	0.007	0/6
Bilobar involvement (absent vs present)	3.2 (1.6–6.6)	<0.001	–	–	–	–
Internal artery (absent vs present) ^c	8.2 (4.8–14.0)	<0.001	3.0 (1.5–5.9)	1.09	0.002	0/7
Two-trait predictor of venous invasion ^{c,d}	7.0 (3.9–12.4)	<0.001	–	–	–	–
Complete “capsule” (absent vs present)	0.08 (0.04–0.2)	<0.001	–	–	–	–
Non-smooth tumour margin (absent vs present)	10.6 (5.9–18.9)	<0.001	4.4 (2.2–8.6)	1.48	<.001	0/10
HCC growth subtype (single nodular vs single nodular with extranodular growth vs confluent multinodular)	3.4 (2.3–4.8)	<0.001	–	–	–	–

Note: Unless stated otherwise, data in parentheses are 95% confidence intervals.

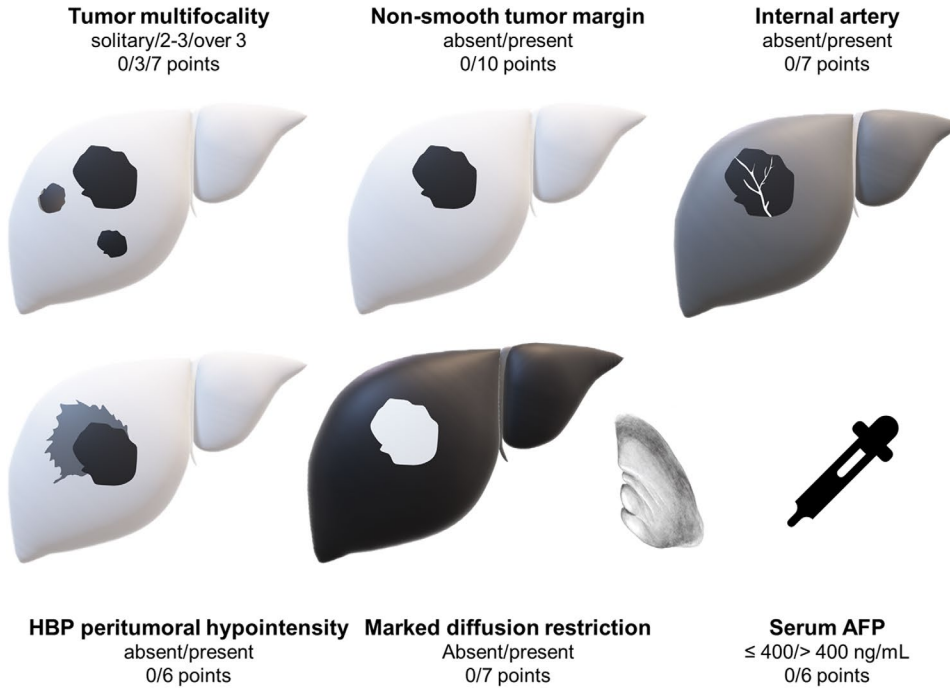
Abbreviations: AFP, alpha-fetoprotein; AST, aspartate aminotransferase; BCLC, Barcelona Clinic Liver Cancer; MVI, microvascular invasion; PLT, platelet count.

^aSolitary tumour corresponded to 0 point, 2–3 tumours corresponded to 3 points, whilst > 3 tumours corresponded to 7 points.

^bDue to significant collinearity (Spearman's rho = 0.611, 95% confidence interval: 0.537–0.675, $P < .001$), “hepatobiliary phase peritumoral hypointensity” was chosen to fit into the multivariable logistic regression model because of the larger odds ratio.

^cDue to significant collinearity (Spearman's rho = 0.841, 95% confidence interval: 0.805–0.870, $P < .001$), the ‘internal artery’ was chosen to fit into the multivariable logistic regression model because of the larger odds ratio.

^dTwo-trait predictor of venous invasion is based on the combination of two imaging features: ‘internal artery’ and ‘hypointense halo evaluated in the portal venous or equilibrium phases’.¹³



Tumor multifocality	Number of definite intrahepatic HCC lesions with characteristic enhancement pattern (stars)	
Non-smooth tumor margin	Non-nodular tumors or nodular tumors with irregular margin and budding portion at the tumor periphery in any imaging plane (star).	
Internal artery	Presence of discrete arterial enhancement within the tumor. <i>T1-weighted arterial phase (right) image demonstrates presence of artery (arrow) within the tumor in relative to the pre-contrast (left) image.</i>	
HBP peritumoral hypointensity	Presence of wedge-shaped or flame-like hypointense area adjacent to the tumor border on hepatobiliary phase images (star).	
Marked diffusion restriction	Increased signal intensity of the liver observation at diffusion-weighted imaging in relative to the spleen, not solely attributable to T2-weighted imaging shine-through effect. <i>Diffusion-weighted imaging (b=1200 s/mm², left) and apparent diffusion coefficient map (right) show a tumor (star) with marked restricted diffusion in comparison to the spleen (arrow).</i>	

FIGURE 2 Graphical illustration of the MVI score

TABLE 3 Testing centre predictive performances for microvascular invasion based on consensus interpretations

	AUC	Sensitivity	Specificity	PPV	NPV	Accuracy
MVI score						
Whole cohort						
Optimal model (>20 points)	0.800 (0.707–0.874)	23/44 (52)	48/54 (89)	23/29 (79)	48/69 (70)	71/98 (72)
High sensitivity model (>12 points)		39/44 (89)	27/54 (50)	39/66 (59)	27/32 (84)	66/98 (67)
High specificity model (>26 points)		12/44 (27)	54/54 (100)	12/12 (100)	54/86 (63)	66/98 (67)
BCLC-0/A patients						
Optimal model (>20 points)	0.726 (0.609–0.824)	8/24 (33)	43/49 (88)	8/14 (57)	43/59 (73)	51/73 (70)
High sensitivity model (>12 points)		20/24 (83)	27/49 (55)	20/42 (48)	27/31 (87)	47/73 (64)
High specificity model (>26 points)		1/24 (4)	49/49 (100)	1/1 (100)	49/72 (68)	50/73 (68)
BCLC-B patients						
Optimal model (>20 points)	0.875 (0.682–0.972)	15/20 (75)	5/5 (100)	15/15 (100)	5/10 (50)	20/25 (80)
High sensitivity model (>12 points)		19/20 (95)	0/5 (0)	19/24 (79)	0/1 (0)	19/25 (76)
High specificity model (>26 points)		11/20 (55)	5/5 (100)	11/11 (100)	5/14 (36)	16/25 (64)
MVI predictive models proposed by Renzulli et al. ^{13a}						
Whole cohort						
At least two features present (optimal model)	0.648 (0.545–0.742)	23/44 (52)	42/54 (78)	23/35 (66)	42/63 (67)	65/98 (66)
At least one feature present (high sensitivity model)		42/44 (95)	0/54 (0)	42/96 (44)	0/2 (0)	42/98 (43)
All three features present (high specificity model)		8/44 (18)	53/54 (98)	8/9 (89)	53/89 (60)	61/98 (62)
BCLC-0/A patients						
At least two features present (optimal model)	0.599 (0.478–0.712)	10/24 (42)	40/49 (82)	10/19 (53)	40/54 (74)	50/73 (68)
At least one feature present (high sensitivity model)		23/24 (96)	0/49 (0)	23/72 (32)	0/1 (0)	23/73 (32)
All three features present (high specificity model)		1/24 (4)	48/49 (98)	1/2 (50)	48/71 (68)	49/73 (67)
BCLC-B patients						
At least two features present (optimal model)	0.620 (0.406–0.805)	13/20 (65)	2/5 (40)	13/16 (81)	2/9 (22)	15/25 (60)
At least one feature present (high sensitivity model)		19/20 (95)	0/5 (0)	19/24 (79)	0/1 (0)	19/25 (76)
All three features present (high specificity model)		7/20 (35)	5/5 (100)	7/7 (100)	5/18 (28)	12/25 (48)

TABLE 3 (Continued)

	AUC	Sensitivity	Specificity	PPV	NPV	Accuracy
MVI predictive model proposed by Min et al. ^{6b}						
Whole cohort						
Five-point scale (score ≥ 4)	0.684 (0.582–0.774)	10/44 (23)	51/54 (94)	10/13 (77)	51/85 (60)	61/98 (62)
BCLC-0/A patients						
Five-point scale (score ≥ 4)	0.610 (0.488–0.722)	2/24 (8)	47/49 (96)	2/4 (50)	47/69 (68)	49/73 (67)
BCLC-B patients						
Five-point scale (score ≥ 4)	0.685 (0.470–0.854)	8/20 (40)	4/5 (80)	8/9 (89)	4/16 (25)	12/25 (48)
MVI predictive models proposed by Lee et al. ^{14c}						
Whole cohort						
Combination of any two reported findings	0.658 (0.556–0.751)	24/44 (55)	43/54 (80)	24/35 (69)	43/63 (68)	67/98 (68)
Combination of all three reported findings		9/44 (20)	51/54 (94)	9/12 (75)	51/86 (59)	60/98 (61)
BCLC-0/A patients						
Combination of any two reported findings	0.599 (0.477–0.712)	10./24 (42)	40/49 (82)	10/19 (53)	40/54 (74)	50/73 (68)
Combination of all three reported findings		2/24 (8)	47/49 (96)	2/4 (50)	47/69 (68)	49/73 (67)
BCLC-B patients						
Combination of any two reported findings	0.635 (0.420–0.816)	14/20 (70)	3/5 (60)	14/16 (88)	3/9 (33)	17/25 (68)
Combination of all three reported findings		7/20 (35)	4/5 (80)	7/8 (88)	4/17 (24)	11/25 (44)

Note: Unless stated otherwise, data in parentheses are 95% confidence intervals or percentages. AUC was measured according to the MVI scoring systems, whilst the remaining diagnostic estimates were computed based on binary scales.

Abbreviations: AUC, area under the receiver operating curve; PPV, positive predictive value; NPV, negative predictive value; MVI, microvascular invasion; NA, not applicable.

^aThe imaging findings reported by Renzulli et al. included peritumoral enhancement (equal to “corona enhancement” in the current study), non-smooth tumour margin, and the two-trait predictor of venous invasion.

^bThe imaging features reported by Min et al. included non-smooth tumour margin, irregular rim-like enhancement on arterial phase, peritumoral arterial phase hyperenhancement, and peritumoral hepatobiliary phase hypointensity.

^cThe imaging findings reported by Lee et al. included arterial peritumoral enhancement, non-smooth tumour margin, and hepatobiliary phase peritumoral hypointensity.

CI: 0.545–0.742, $P = .003$), Min et al. (0.684, 95%CI: 0.582–0.774, $P = .03$), and Lee et al. (0.658, 95% CI: 0.556–0.751, $P = .006$) (Figure 3).

All binary diagnostic estimates of our MVI models were trend-wise superior to previous MVI schemes, but statistically significant difference was detected between our MVI score-based optimal model (>20 points) and Lee’s optimal model in accuracy (72% vs. 68%, $P < .001$, entire testing centre cohort); and between our MVI score-based high sensitivity model (>12 points) and Renzulli’s high sensitivity model in accuracy (67% vs. 43%, $P < .001$, entire testing centre cohort; 64% vs. 32%, $P < .001$, BCLC 0/A patients) and specificity (50% vs. 0%, $P < .001$, entire testing centre cohort; 55% vs. 0%, $P < .001$, BCLC 0/A patients).

3.3 | Survival Analysis

Survival outcomes are summarized in Table 4 and plotted as the Kaplan–Meier curves in Figure 4.

Median follow-up was 29.0 months (95% CI: 15.0–36.0). A total of 238 (75%) and 281 (88%) patients had complete RFS and OS information, respectively, and were included in the survival analyses. Amongst them, 95 (40%) patients experienced tumour recurrence, and 41 (15%) patients died. Median OS was not reached, whilst mean OS was 53.2 months (95% CI: 50.3–56.2). Median RFS was 32.0 months (95% CI: 25.0–50.0).

Patients with pathologically confirmed MVI had significantly shorter OS (61.0 months vs. not reached, $P < .001$) and

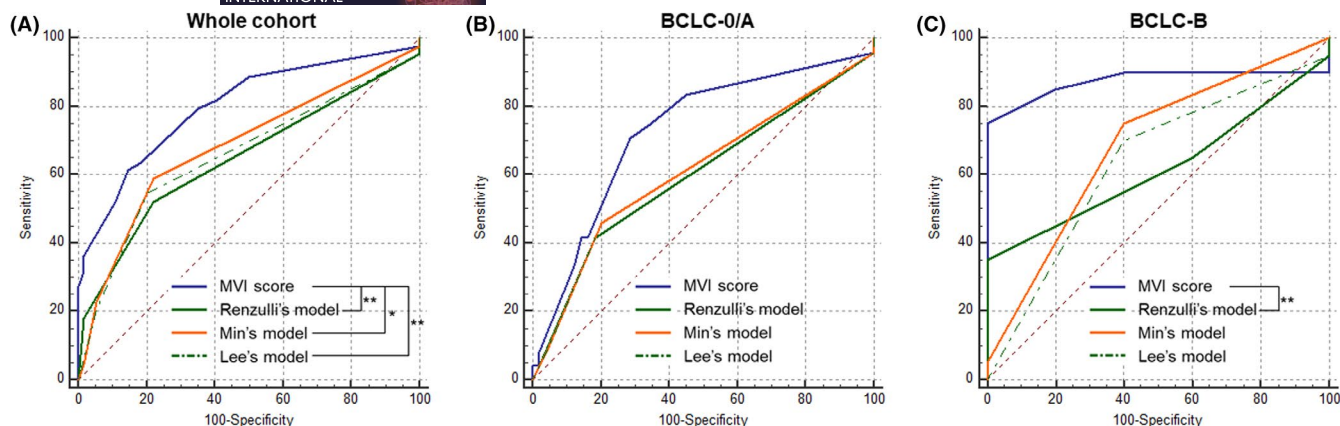


FIGURE 3 Receiver operating curves of the MVI predictive systems for the testing centre data based on the whole cohort (A), patients with Barcelona Clinic Liver Cancer stage 0/A tumours (B), and those with Barcelona Clinic Liver Cancer stage B tumours (C). * $P < .05$, ** $P < .01$

RFS (12.0 months vs. 50.0 months, $P < .001$) than those without MVI. Similarly, based on our optimal model, patients with model predicted MVI had significantly shorter OS (61.0 months vs. not reached, $P < .001$) and RFS (13.0 months vs. 42.0 months, $P < .001$) than those without. Based on the MVI risk system, patients at high risk for MVI had a significantly shorter OS and RFS compared with those at low or medium risks (all $P < .001$), but no difference in OS ($P = .13$) or RFS ($P = .59$) was detected between the low and medium-risk groups.

Pathological confirmation of MVI (C-index for OS, 0.715; C-index for RFS, 0.684), the optimal model-predicted MVI (C-index for OS, 0.700; C-index for RFS, 0.652) and the MVI risk system (C-index for OS, 0.762; C-index for RFS, 0.708) demonstrated comparable performances in predicting OS ($P = .31$ to $.99$) and RFS ($P = .09$ to 1.00).

4 | DISCUSSION

MVI has been widely accepted as an independent risk factor for poorer prognosis in HCC,¹⁻⁵ but its visualization is beyond current imaging resolutions.^{4,6,8-20} In this dual-centre study, we developed and externally validated an MVI score based on serum AFP and five EOB-MR imaging features. This scoring system demonstrated superior predictive performances compared with previous MVI schemes in an independent testing dataset and achieved accurate postoperative survival stratification.

MVI is a promising decision-making biomarker to be incorporated into current HCC staging systems,¹⁻⁵ on the premise of accurate and reliable preoperative MVI prediction. Based on the external testing centre data, our MVI score demonstrated superior AUCs and binary diagnostic performances than existing models^{6,13,14} throughout all BCLC stages, though the testing centre sample size ($n = 98$) may have been inadequate to obtain the substantial statistical difference. These improvements were largely achieved due to the use of as many as 38 candidate MR imaging features, including those related to the liver parenchyma (cirrhosis), tumour burden (tumour

multiplicity, size, bilobar involvement, etc.), tumour characteristics (LI-RADS features, internal artery, HCC growth subtype, etc.) and the tumour periphery (corona enhancement, PVP and HBP peritumoral hypointensity, etc.), in contrast to previous studies which included a limited number (typically <10) of imaging features.^{4,6,8-20,30} Expectedly, as observed for all evaluated MVI schemes, the model performances dropped in patients with BCLC 0/A tumours compared with those with BCLC B tumours, highlighting the challenges to detect MVI in earlier stage tumours. Of note, despite substantial inter-rater agreement on the MVI score, the agreement on all binary models was moderate. These findings were in consistent with Min et al.'s results,⁶ and underscored the need to further minimize interobserver variability before this scoring system could be used as a reliable decision-making tool.

Diffusion restriction is a distinct characteristic of HCC and an expected MVI predictor because MVI is more frequently observed in higher grade HCCs and can lead to a more complex tumour microenvironment,^{16,17,30,31} both could result in diffusion restriction. However, conflicting results have been reported thus far regarding the utilities of restricted diffusion (or lower ADC values) in MVI prediction.^{30,31} In line with a recent meta-analysis,³⁰ diffusion restriction, in general, was not associated with MVI in our study, as 100% of HCCs demonstrated some degree of restricted diffusion, regardless of MVI status. Nevertheless, marked diffusion restriction, which could be easily assessed by comparing the extent of tumour diffusion restriction to that of the spleen, was significantly associated with MVI. Therefore, this readily-assessed feature could provide important information regarding the extent of restriction diffusion in routine practice, without the requirement for complex quantitative analyses.

Tumour multifocality was another significant predictor for MVI in our study, despite its controversial role elsewhere. Chandarana et al.³² and Lei et al.⁸ found tumour multifocality as significantly associated with MVI, whilst others reported no significant correlations between this feature and MVI.^{4,6,13,14} However, tumour multifocality was pooled to be significantly predictive of MVI in Hong et al.'s

TABLE 4 Survival analysis outcomes

	Overall survival (months)	P value	C-index	Recurrence-free survival (months)	P value	C-index
All patients	53.2 (50.3–56.2)	–	–	32.0 (25.0–50.0)	–	–
Pathologically confirmed MVI						
MVI positive	61.0 (42.0–61.0)	<.001	0.715 (0.632–0.798)	12.0 (9.0–25.0)	<.001	0.684 (0.625–0.743)
MVI negative	Not reached			50.0 (39.0–50.0)		
Optimal model based on the MVI score						
Model-predicted positive (>20 points)	61.0 (42.0–61.0)	<.001	0.700 (0.603–0.797)	13.0 (8.0–28.0)	<.001	0.652 (0.588–0.716)
Model-predicted negative (≤20 points)	Not reached			42.0 (36.0–50.0)		
Risk system based on the MVI score						
Low risk (≤12 points)	Not reached	<.001	0.762 (0.679–0.845)	Not reached	<.001	0.708 (0.649–0.767)
Medium risk (13–26 points)	Not reached			42.0 (25.0–44.0)		
High risk (>26 points)	36.0 (22.0–61.0)			7.0 (5.0–12.0)		

Note: Unless stated otherwise, data are presented as median (95% confidence intervals).

Data are mean (95% confidence intervals) because the median time was not reached.

Abbreviation: MVI, microvascular invasion.

meta-analysis.³⁰ Multiple tumours in MVI-positive patients might be a result of increased intrahepatic tumour spreading through microvascular structures.³³ On the contrary, both MVI and multifocality are associated with a more aggressive tumour biological behaviour.^{30,32}

In accordance with prior works, non-smooth tumour margin,^{13,14,23} HBP peritumoral hypointensity^{4,14} and internal arteries^{13,28} were also significantly associated with MVI in this study. The underlying biological correlations between these features and MVI have been extensively explored.^{11,13,14,28,34,35} Specifically, non-smooth tumour margin has been associated with more aggressive tumour growth patterns and increased MVI.³⁴ HBP peritumoral hypointensity could be explained by the impaired functions of the peritumoral hepatocyte organic anion-transporting polypeptide transporters following the perfusion alterations induced by MVI.^{11,14} Additionally, the presence of internal arteries may indicate markedly increased angiogenesis and has been found to correlate with a distinct HCC molecular subtype with increased cell proliferation, matrix invasion and MVI.^{13,28,35}

For postoperative survival stratification, histologic MVI was found significantly correlated with poorer postoperative prognosis in the current study, which was in line with previous reports.^{1–5} Similarly, derived from the MVI score, both the binary optimal model and the categorical risk system could effectively stratify postoperative RFS and OS, with comparable performances as histologic MVI, highlighting the potential of our proposed MVI score in predicting postoperative patient prognosis.

Major strengths of the current study constituted the dual-institution design, the inclusion of 417 HCC patients, and evaluations of the largest number of EOB-MRI features for MVI to date. Furthermore, we conducted head-to-head comparisons with several previously reported MVI models in an independent dataset, providing a direct assessment of the relative performances of these schemes. Our findings were clinically relevant. By identifying patients with MVI in the pretreatment stage, the proposed scoring system may open new scenarios for choosing amongst different therapeutic regimens (e.g. orient toward more aggressive surgical approaches or larger ablated areas and prioritize adjuvant intraarterial or systematic therapies), tailor follow-up strategies with more sensitive techniques and shorter time intervals (e.g. EOB-MRI over CT),³⁶ and help stratifying prognosis.

This study had several limitations. First, the retrospective nature could have introduced substantial selection biases. Second, patients with macrovascular invasion at imaging were included in the training centre to guarantee enough positive cases for effective modelling.²⁵ However, the clinical relevance of identifying MVI in this population is limited as in theory most (if not all) of these patients would have MVI. Therefore, we excluded these patients from the testing centre dataset to avoid overestimation of model performances and achieve more rigorous model validation. Nevertheless, this design may have exacerbated the discrepancies in patient characteristics between the training and testing centres. Third, the prevalence of MVI was higher than several previous studies,^{2–6,8–10,12–14,20,23} which might

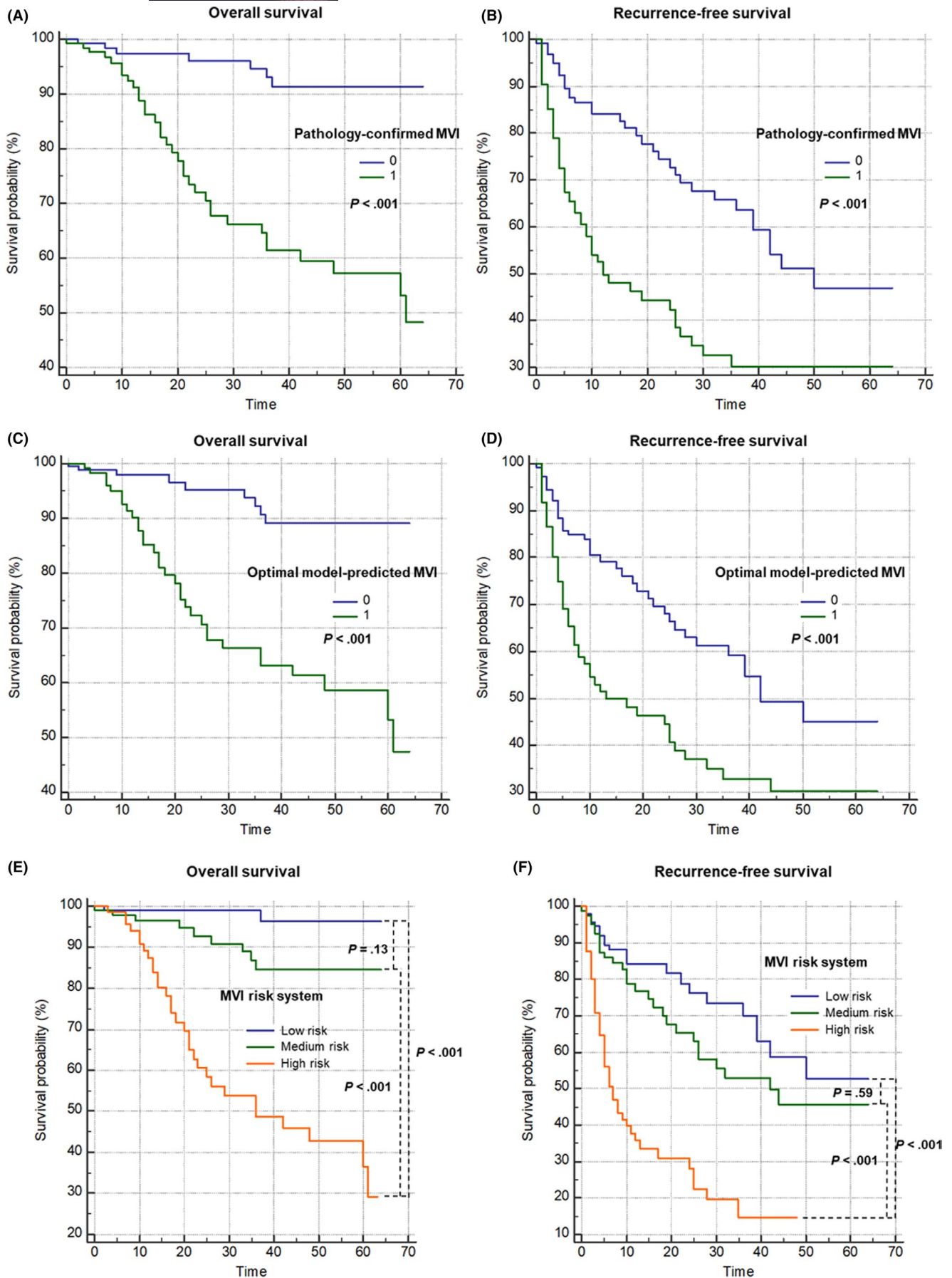


FIGURE 4 The Kaplan-Meier curves of pathologically-confirmed MVI (A, B), optimal model-predicted MVI (C, D), and the MVI risk system (E, F) based on the training centre data

have impacted the diagnostic performances of our proposed MVI score. Fourth, all imaging evaluations were conducted centrally by only two reviewers, which dampened the generalizability of our results. Fifth, clinical outcome data were not available for the testing centre. Finally, all MR images were acquired with EOB based on routine clinical sequences without consideration of advanced quantitative MR imaging techniques.^{16,17,37} However, as HBP images can only be acquired with EOB-MRI, the feature HBP peritumoral hypointensity is not measurable with extracellular contrast agents-enhanced MRI. Therefore, further fine-tuning on extracellular contrast agents-enhanced MRI is warranted to extrapolate our findings.

In conclusion, in this dual-institution study, we developed and validated an easy-to-use MVI score based on serum AFP and five EOB-MR imaging features in HCC patients. This scoring system allowed accurate preoperative MVI prediction and postoperative survival stratifications thus may help tailor personalized treatment decision-making.

CONFLICT OF INTEREST

All authors disclose no conflict of interest relevant to this work.

DATA AVAILABILITY STATEMENT

The data that support the findings of this study are available on request from the corresponding author.

ORCID

Hanyu Jiang  <https://orcid.org/0000-0002-7726-1618>

Jie Tian  <https://orcid.org/0000-0003-0498-0432>

REFERENCES

- European Association for the Study of the Liver. EASL Clinical Practice Guidelines: Management of hepatocellular carcinoma. *J Hepatol*. 2018;69(1):182-236.
- Lim KC, Chow PK, Allen JC, et al. Microvascular invasion is a better predictor of tumor recurrence and overall survival following surgical resection for hepatocellular carcinoma compared to the Milan criteria. *Ann Surg*. 2011;254:108-113.
- Chan AWH, Zhong J, Berhane S, et al. Development of pre and post-operative models to predict early recurrence of hepatocellular carcinoma after surgical resection. *J Hepatol*. 2018;69(6):1284-1293.
- Lee S, Kang TW, Song KD, et al. Effect of microvascular invasion risk on early recurrence of hepatocellular carcinoma after surgery and radiofrequency ablation. *Ann Surg*. 2021;273(3):564-571.
- Mazzaferro V, Llovet JM, Miceli R, et al. Predicting survival after liver transplantation in patients with hepatocellular carcinoma beyond the Milan criteria: a retrospective, exploratory analysis. *Lancet Oncol*. 2009;10(1):35-43.
- Min JH, Lee MW, Park HS, et al. Interobserver variability and diagnostic performance of gadoxetic acid-enhanced mri for predicting microvascular invasion in hepatocellular carcinoma. *Radiology*. 2020;297(3):573-581.
- Chan ACY, Fan ST, Poon RTP, et al. Evaluation of the seventh edition of the American Joint Committee on Cancer tumour-node-metastasis (TNM) staging system for patients undergoing curative resection of hepatocellular carcinoma: implications for the development of a refined staging system. *HPB*. 2013;15:439-448.
- Lei Z, Li J, Wu D, et al. Nomogram for preoperative estimation of microvascular invasion risk in hepatitis B virus-related hepatocellular carcinoma within the Milan Criteria. *JAMA*. 2016;151(4):356-363.
- Pote N, Cauchy F, Albuquerque M, et al. Performance of PIVKA-II for early hepatocellular carcinoma diagnosis and prediction of microvascular invasion. *J Hepatol*. 2015;62:848-854.
- McHugh PP, Gilbert J, Vera S, et al. Alpha-fetoprotein and tumour size are associated with microvascular invasion in explanted livers of patients undergoing transplantation with hepatocellular carcinoma. *HPB (Oxford)*. 2010;12:56-61.
- Kim KA, Kim MJ, Jeon HM, et al. Prediction of microvascular invasion of hepatocellular carcinoma: usefulness of peritumoral hypointensity seen on gadoxetate disodium-enhanced hepatobiliary phase images. *J Magn Reson Imaging*. 2012;35(3):629-634.
- Witjes CD, Willemsen FE, Verheij J, et al. Histological differentiation grade and microvascular invasion of hepatocellular carcinoma predicted by dynamic contrast-enhanced MRI. *J Magn Reson Imaging*. 2012;36(3):641-647.
- Renzulli M, Brocchi S, Cucchetti A, et al. Can current preoperative imaging be used to detect microvascular invasion of hepatocellular carcinoma? *Radiology*. 2016;279(2):432-442.
- Lee S, Kim SH, Lee JE, Sinn DH. Preoperative gadoxetic acid-enhanced MRI for predicting microvascular invasion in patients with single hepatocellular carcinoma. *J Hepatol*. 2017;67(3):526-534.
- Chen J, Zhou J, Kuang S, et al. Liver imaging reporting and data system category 5: MRI predictors of microvascular invasion and recurrence after hepatectomy for hepatocellular carcinoma. *Am J Roentgenol*. 2019;213(4):821-830.
- Wang WT, Yang L, Yang ZX, et al. Assessment of microvascular invasion of hepatocellular carcinoma with diffusion kurtosis imaging. *Radiology*. 2018;286(2):571-580.
- Wei Y, Huang Z, Tang H, et al. IVIM improves preoperative assessment of microvascular invasion in HCC. *Eur Radiol*. 2019;29(10):5403-5414.
- Granata V, Fusco R, Setola SV, et al. Microvascular invasion and grading in hepatocellular carcinoma: correlation with major and ancillary features according to LIRADS. *Abdom Radiol (NY)*. 2019;44(8):2788-2800.
- Lee S, Kim SH, Hwang JA, Lee JE, Ha SY. Pre-operative ADC predicts early recurrence of HCC after curative resection. *Eur Radiol*. 2019;29(2):1003-1012.
- Sun SW, Sun SW, Xu X, Zhu FP, Zhang YD, Liu XS. Direct comparison of four presurgical stratifying schemes for prediction of microvascular invasion in hepatocellular carcinoma by gadoxetic acid-enhanced MRI. *J Magn Reson Imaging*. 2020;52(2):433-447.
- Yang L, Gu D, Wei J, et al. A radiomics nomogram for preoperative prediction of microvascular invasion in hepatocellular carcinoma. *Liver Cancer*. 2019;8(5):373-386.
- Ma X, Wei J, Gu D, et al. Preoperative radiomics nomogram for microvascular invasion prediction in hepatocellular carcinoma using contrast-enhanced CT. *Eur Radiol*. 2019;29(7):3595-3605.
- Xu X, Zhang HL, Liu QP, et al. Radiomic analysis of contrast-enhanced CT predicts microvascular invasion and outcome in hepatocellular carcinoma. *J Hepatol*. 2019;70(6):1133-1144.
- Wei J, Jiang H, Zeng M, et al. Prediction of microvascular invasion in hepatocellular carcinoma via deep learning: a multi-center and prospective validation study. *Cancers (Basel)*. 2021;13(10):2368.
- Moons KG, Altman DG, Reitsma JB, et al. Transparent reporting of a multivariable prediction model for individual prognosis or diagnosis (TRIPOD): explanation and elaboration. *Ann Intern Med*. 2015;162(1):W1-W73.
- CT/MRI Liver Imaging Reporting and Data System version 2018. American College of Radiology Web site. <https://www.acr.org/Clinical-Resources/Reporting-andData-Systems/LI-RADS/CTMRI-LI-RADS-v2018>. Accessed 1 December 2018.

27. Rhee H, Chung T, Yoo JE, et al. Gross type of hepatocellular carcinoma reflects the tumor hypoxia, fibrosis, and stemness-related marker expression. *Hepatol Int*. 2020;14(2):239-248.
28. Banerjee S, Wang DS, Kim HJ, et al. A computed tomography radiogenomic biomarker predicts microvascular invasion and clinical outcomes in hepatocellular carcinoma. *Hepatology*. 2015;62(3):792-800.
29. Rodriguez-Peralvarez M, Luong TV, Andreana L, et al. A systematic review of microvascular invasion in hepatocellular carcinoma: diagnostic and prognostic variability. *Ann Surg Oncol*. 2013;20:325-339.
30. Hong SB, Choi SH, Kim SY, Shim JH, Lee SS, Byun JH. MRI features for predicting microvascular invasion of hepatocellular carcinoma: a systematic review and meta-analysis. *Liver Cancer*. 2021;10(2):94-106.
31. Surov A, Pech M, Omari J, et al. Diffusion-weighted imaging reflects tumor grading and microvascular invasion in hepatocellular carcinoma. *Liver Cancer*. 2021;10(1):10-24.
32. Chandarana H, Robinson E, Hajdu CH, Drozhinin L, Babb JS, Taouli B. Microvascular invasion in hepatocellular carcinoma: is it predictable with pretransplant MRI? *Am J Roentgenol*. 2011;196(5):1083-1089.
33. Nakashima Y, Nakashima O, Tanaka M, Okuda K, Nakashima M, Kojiro M. Portal vein invasion and intrahepatic micrometastasis in small hepatocellular carcinoma by gross type. *Hepatol Res*. 2003;26(2):142-147.
34. Shimada M, Rikimaru T, Hamatsu T, et al. The role of macroscopic classification in nodulartype hepatocellular carcinoma. *Am J Surg*. 2001;182(2):177-182.
35. Segal E, Sirlin CB, Ooi C, et al. Decoding global gene expression programs in liver cancer by noninvasive imaging. *Nat Biotechnol*. 2007;25(6):675-680.
36. Liu X, Jiang H, Chen J, Zhou Y, Huang Z, Song B. Gadoteric acid disodium-enhanced magnetic resonance imaging outperformed multidetector computed tomography in diagnosing small hepatocellular carcinoma: A meta-analysis. *Liver Transpl*. 2017;23(12):1505-1518.
37. Zeng GL, DiBella EV. Non-iterative image reconstruction from sparse magnetic resonance imaging radial data without priors. *Vis Comput Ind Biomed Art*. 2020;3(1):9.

SUPPORTING INFORMATION

Additional supporting information may be found in the online version of the article at the publisher's website.

How to cite this article: Jiang H, Wei J, Fu F, et al. Predicting microvascular invasion in hepatocellular carcinoma: A dual-institution study on gadoteric acid disodium-enhanced MRI. *Liver Int*. 2022;42:1158-1172. doi: [10.1111/liv.15231](https://doi.org/10.1111/liv.15231)